Electronic Supplementary Material (ESI) for Dalton Transactions.

Supporting information for

# Confining redox-active metal sites in acidic porous scaffolds for catalytic transformation of lignin-derived phenols to naphthenes

Hang Li, Guan-Ze Chen and Chuan-De Wu*

*State Key Laboratory of Silicon and Advanced Semiconductor Materials, Department of Chemistry, Zhejiang University, Hangzhou 310027, P. R. China*

*E-mail: cdwu@zju.edu.cn*

## Experimental

### Materials

High purity chemicals were commercially available and directly used without further purification. Nickel(II) nitrate hexahydrate ($Ni(NO_3)_2 \cdot 6H_2O$, Sinopharm Chemical Reagent Co., Ltd.), tetraethyl orthosilicate (TEOS, Energy Chemical Reagent Co., Ltd.), 2-picolinic acid (>99%, Energy Chemical Reagent Co., Ltd.) and aluminium chloride (>99%, $AlCl_3$, Energy Chemical Reagent Co., Ltd.) were used as received. Guaiacol (>99%), 3-methoxyphenol (>99%), 2,6-dimethoxyphenol (>99%), phenol (>99%), diphenyl ether (>99%) and anisole (>99%) were obtained from Energy Chemical. Pyrocatechol (>99%), resorcinol (>99%) and hydroquinone (>99%) were obtained from Sinopharm Chemical Reagent. 4-Isopropylphenol (>99%) and 3-isopropylphenol (>99%) were obtained from Shanghai Macklin Biochemical. 4,4'-Oxydiphenol (>99%) was obtained from Shanghai Aladdin Biochemical.

### Characterizations

The contents of nickel and aluminum were detected by inductively coupled plasma mass spectrometry (ICP-MS) on PerkinElmer NexION 300X Agilent Technologies 7800 ICP-MS. Thermogravimetric analysis (TGA) experiments were performed on NETZSCH STA 409PC/PG instrument with a heating rate of 10 $^{o}$C/min in an air atmosphere. Fourier transform infrared (FT-IR) spectra were collected on Nicolet NEXUS 470 spectrometry via KBr pellet method.

Powder X-ray diffraction (PXRD) data were recorded on a RIGAKU D/MAX 2550/PC for Cu Kα radiation ($\lambda$ =1.5406 Å) at 40 kV and 30 mA. The scanning angle ($2\theta$) is in the range of 5-90°. A Micromeritics ASAP 2020 surface area analyzer was used to measure $N_2$ gas adsorption/desorption isotherms. The Brunauer-Emmett-Teller (BET) surface area and density functional theory (NLDFT) pore size distribution were estimated on the sorption isotherms. Scanning electron microscopy (SEM) images were recorded on a Hitachi S-4800 equipment. Transmission electron microscopy (TEM) was recorded on a JEM 2100 F equipment.

Hydrogen-temperature programmed reduction ($H_2$-TPR) and $NH_3$-temperature programmed desorption ($NH_3$-TPD) were recorded on VDSorb-91i equipment with a TCD detector. Pyridine adsorption FT-IR spectra (Py-IR) was conducted on a Thermo fisher Nicolet iS50 spectrometer to probe the accessible acid sites. X-ray photoelectron spectra (XPS) were recorded on a VG ESCALAB MARK II machine, and the C 1s peak at 284.8 eV was used to calibrate the binding energies.

Cyclic voltammetry experiments were performed at room temperature with a conventional three-electrode electrochemical cell on a CHI-660E electrochemical workstation (made in Shanghai, China). The three-electrode system used in this work consists of a reticulated vitreous carbon electrode (0.25 $cm^2$, painted by Ni powder or $Al_2O_3$ mixed with nafion and isopropyl alcohol) as the working electrode, a saturated calomel electrode (SCE) as the reference electrode, and a Pt foil auxiliary electrode, which were dipped directly in the electrolyte solution (saturated potassium chloride solution mixed with isopropanol). All potentials were measured and reported with respect to SCE in this paper.

**Figures**

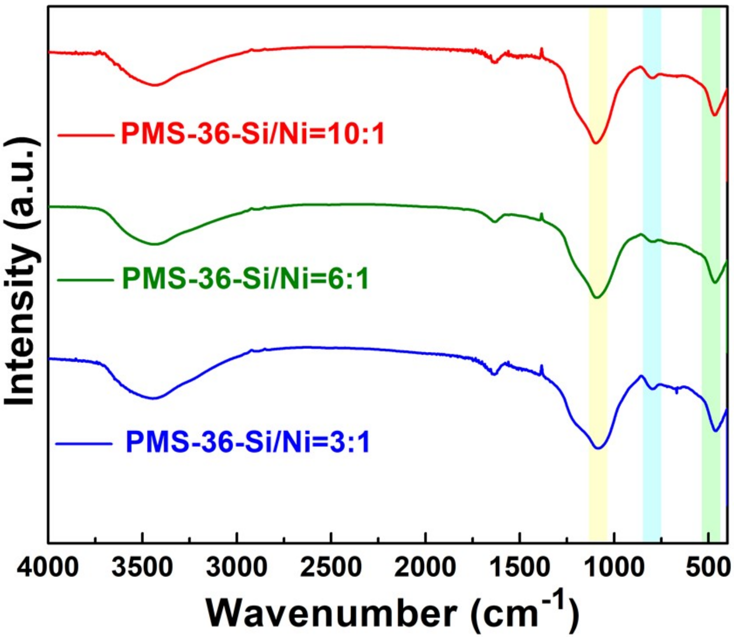

**Fig. S1** FT-IR spectra of the PMS materials with different silicon/nickel ratios.

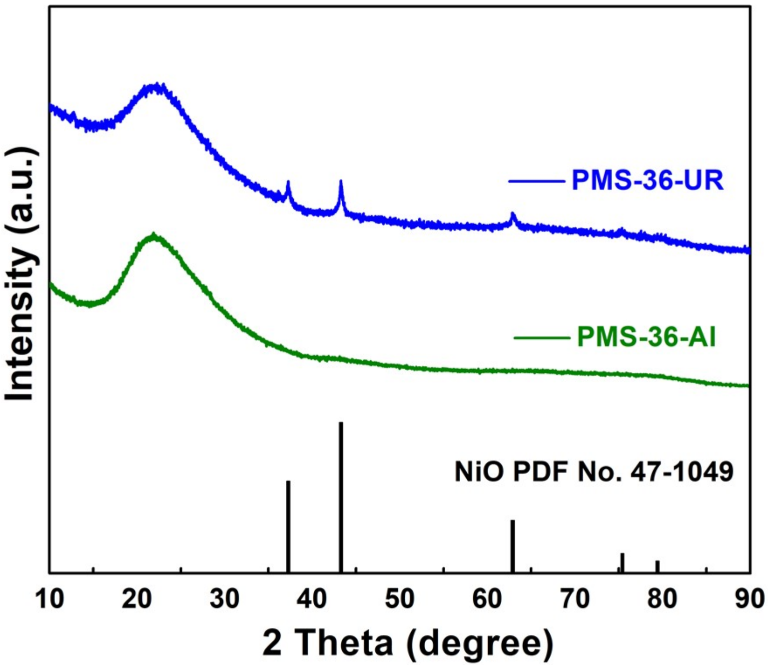

**Fig. S2** PXRD patterns of PMS-36-Al and PMS-36-UR.

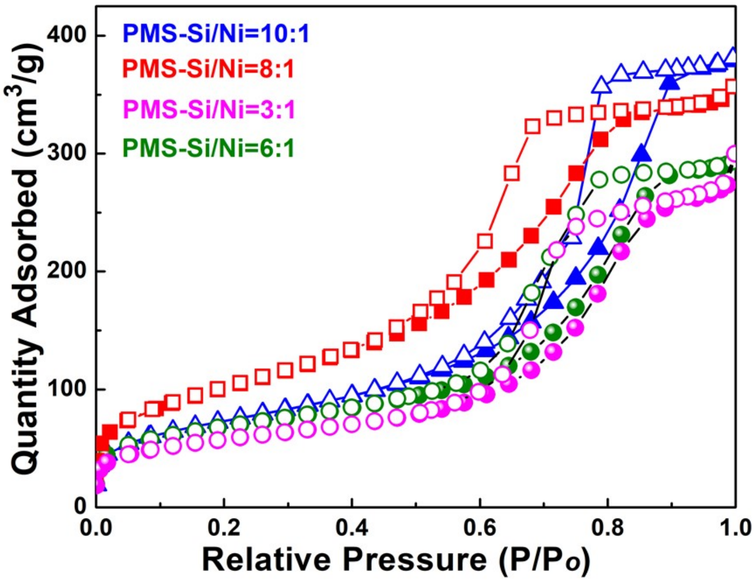

**Fig. S3** $N_2$ sorption isotherms of the PMS materials with different ratios of silicon/nickel.

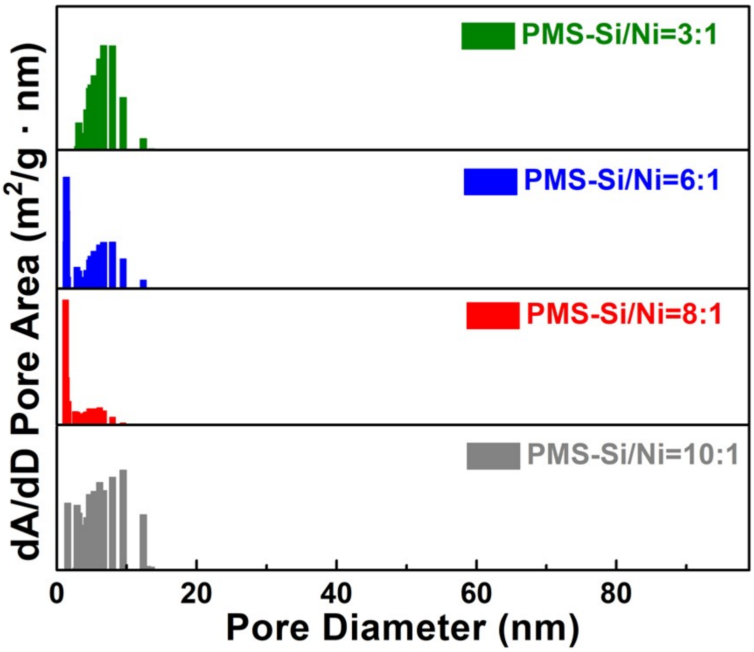

**Fig. S4** Pore size distributions for the PMS materials with different ratios of silicon/nickel.

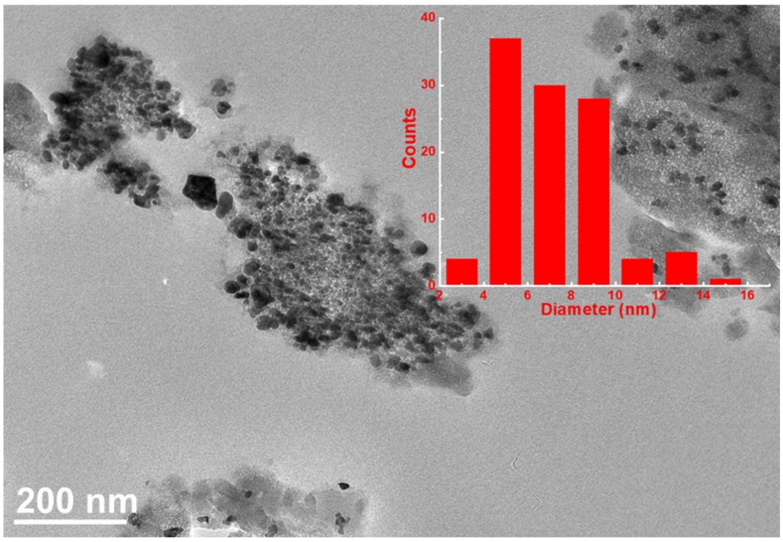

**Fig. S5** TEM image of PMS-36-Ni (the inset shows the size distribution of metal nanoparticles).

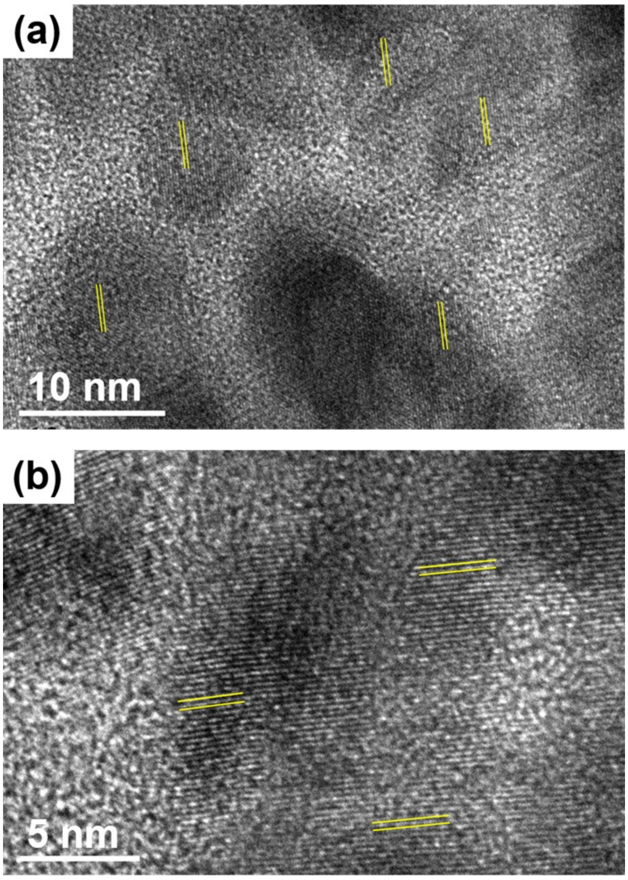

**Fig. S6** HRTEM images of PMS-36.

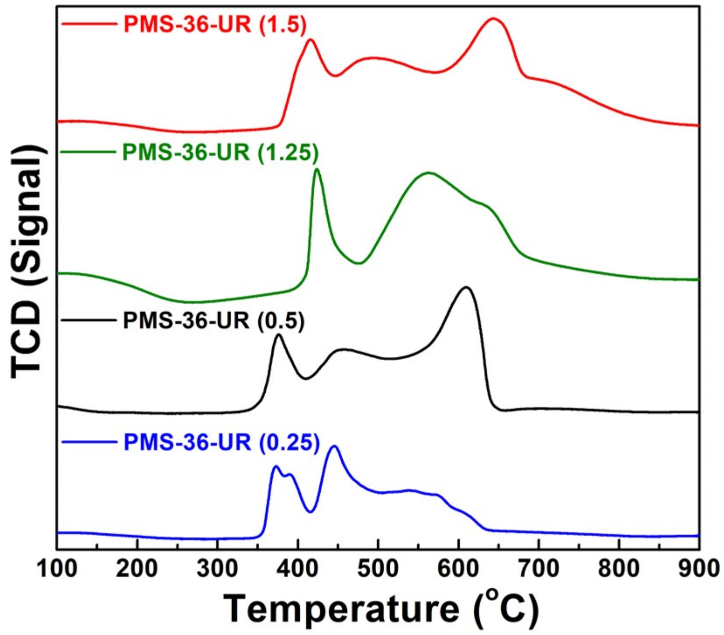

**Fig. S7** $H_2$-TPR profiles of the unreduced PMS materials with different contents of Al (marked as PMS-36-UR (X), where UR and X represent unreduced and Al/Ni ratio, respectively).

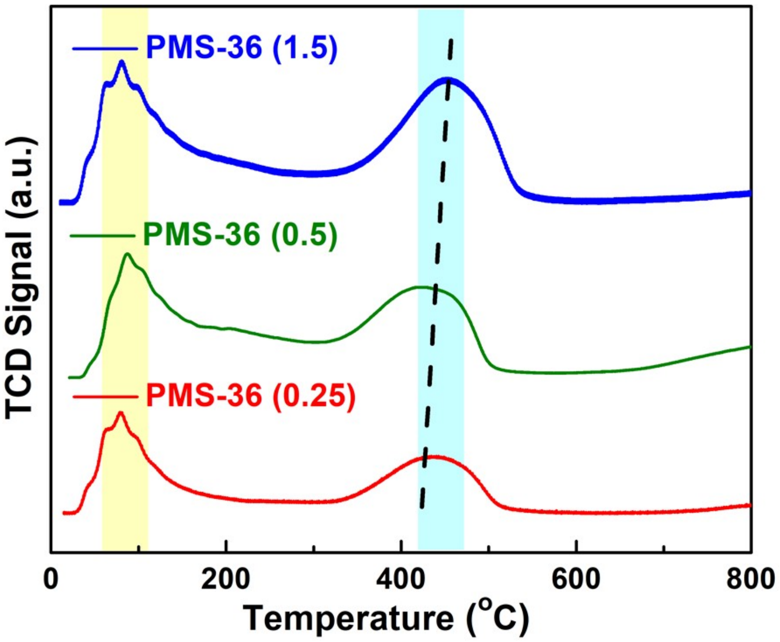

**Fig. S8** $NH_3$-TPD profiles of the PMS materials with different contents of Al (marked as PMS-36 (X), where X represents the ratio of Al/Ni).

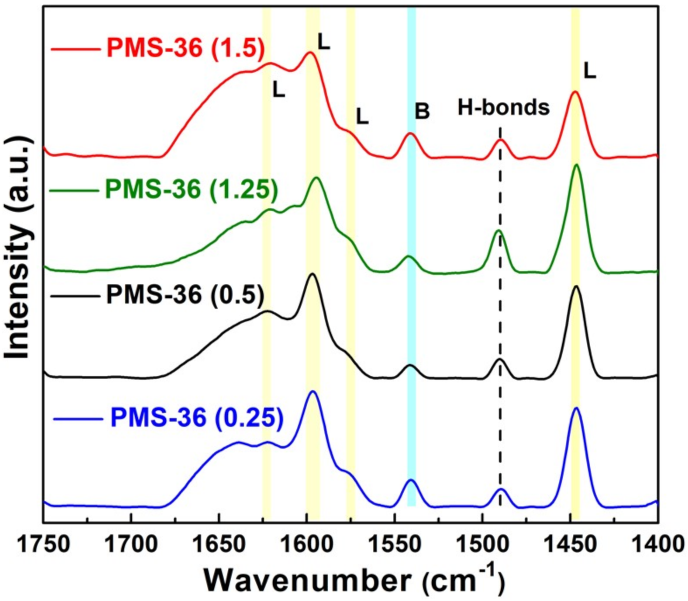

**Fig. S9** Py-IR profiles of the PMS materials with different contents of Al (marked as PMS-36 (X), where X represents the ratio of Al/Ni).

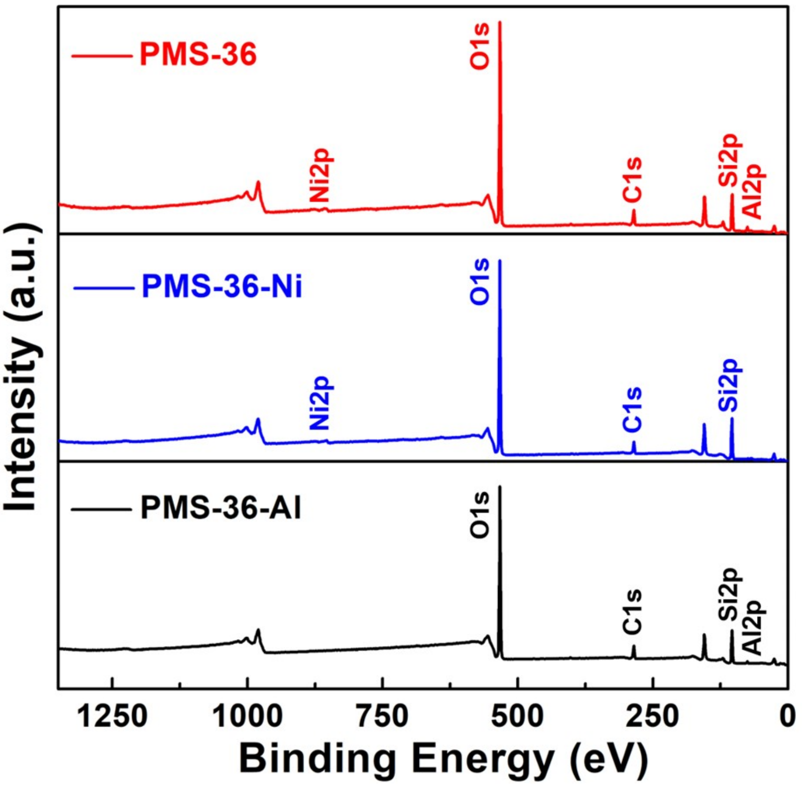

**Fig. S10** XPS profiles of PMS-36, PMS-36-Ni and PMS-36-Al.

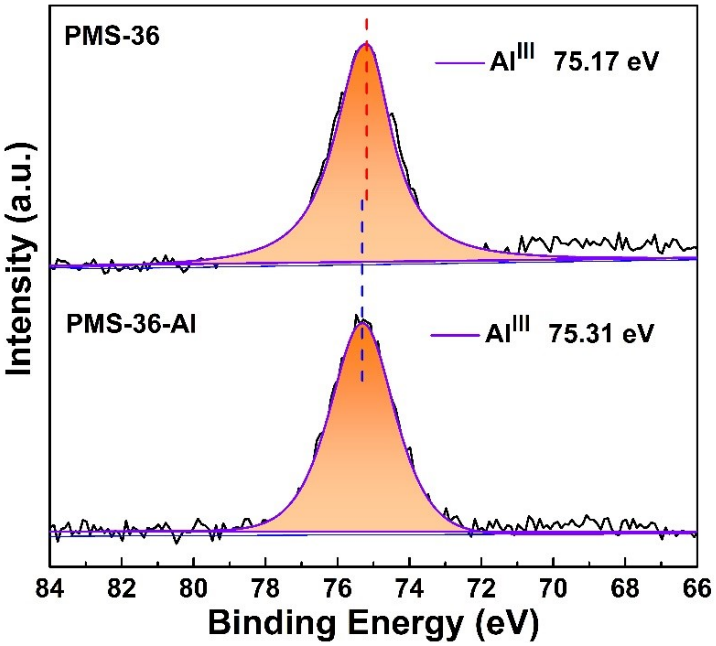

**Fig. S11** High resolution Al 2p XPS spectra of PMS-36 and PMS-36-Al.

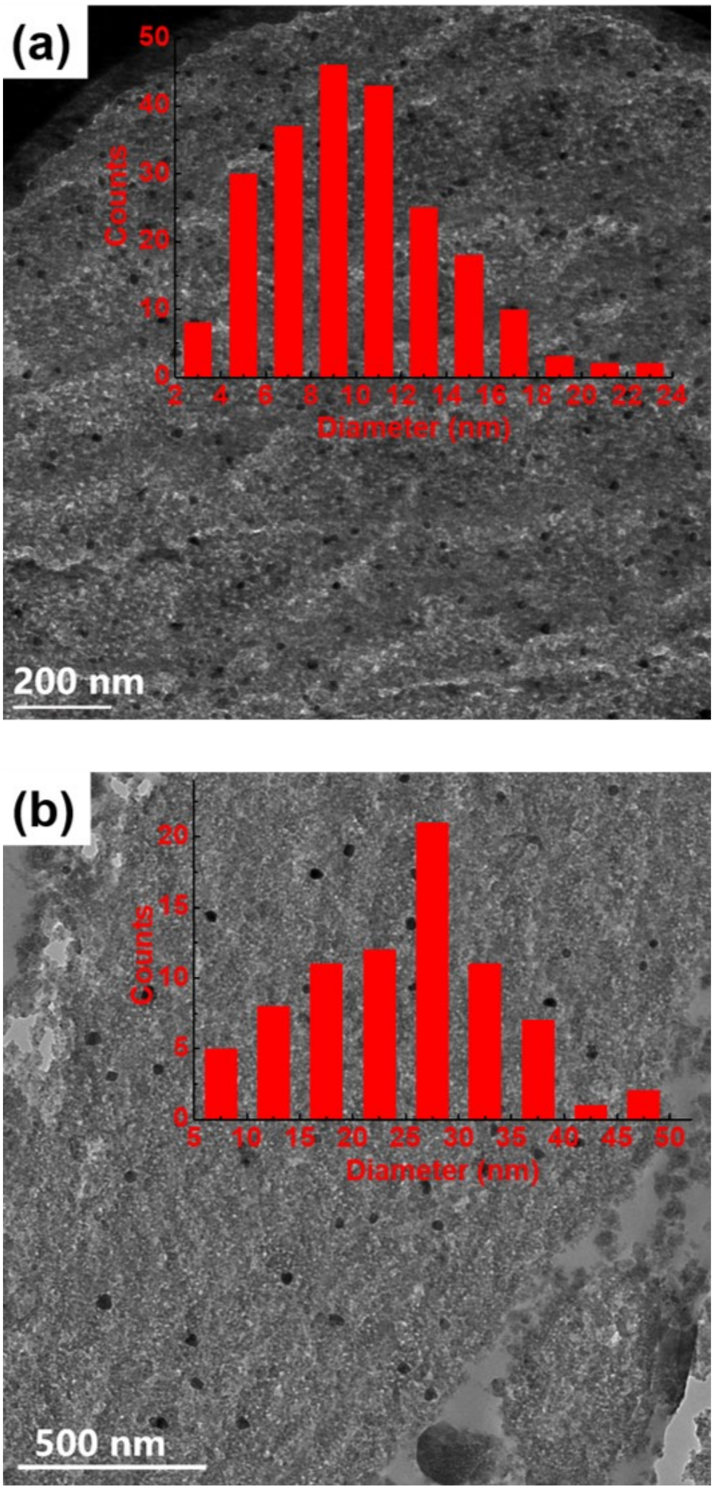

**Fig. S12** TEM images of the PMS materials calcinated at different temperatures. (a) 850 $^{o}$C; (b) 950 $^{o}$C.

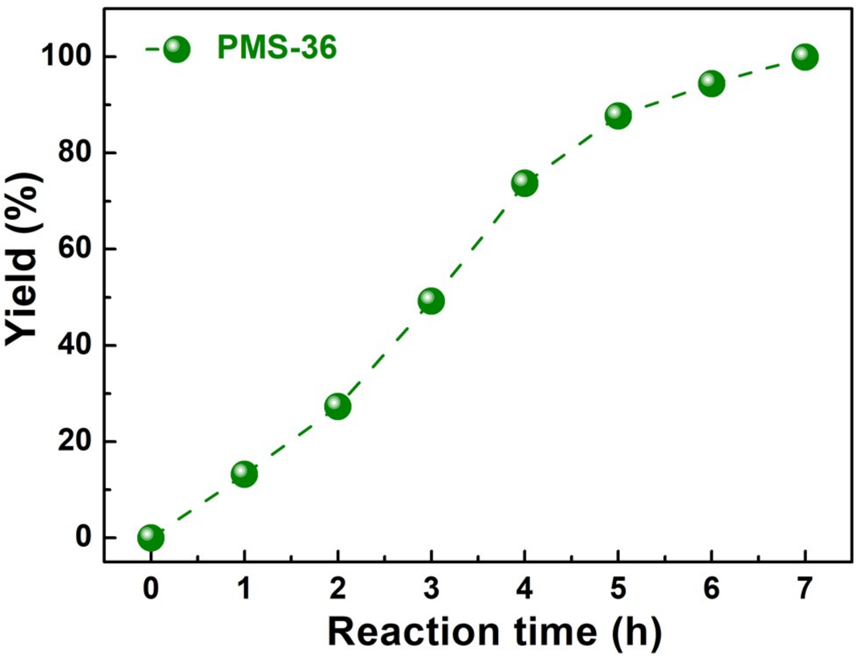

**Fig. S13** Yield of cyclohexane versus reaction time under 2.0 MPa $H_2$ atmosphere catalyzed by PMS-36. Reaction conditions: 0.5 mmol guaiacol, PMS-36 (3.0% mmol, based on Ni), 200 $^oC$.

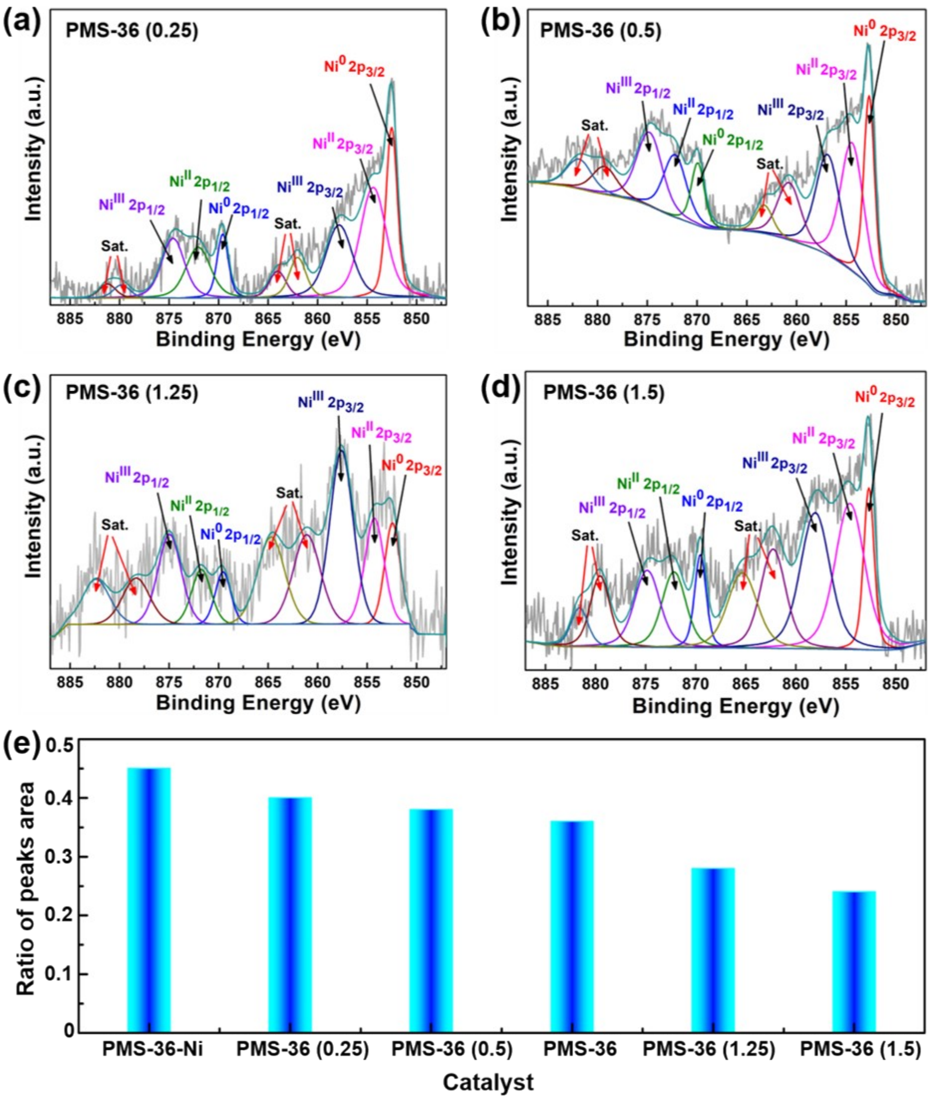

**Fig. S14** Ni 2p peak profiles for (a) PMS-36 (0.25), (b) PMS-36 (0.5), (c) PMS-36 (1.25) and (d) PMS-36 (1.5); (e) the relative ratios of nickel/nickel oxide peaks across variation ratios of Al/Ni.

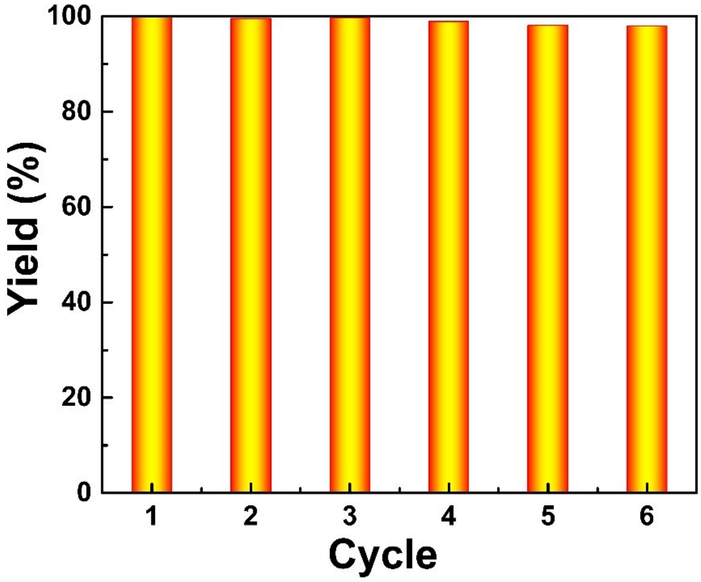

**Fig. S15** The recyclability of PMS-36 for hydrodeoxygenation of guaiacol.

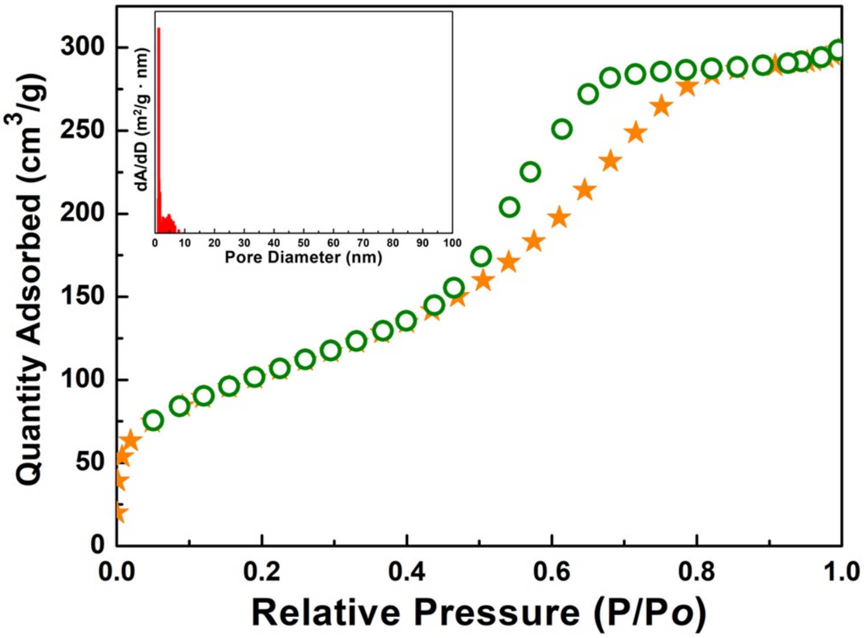

**Fig. S16** $N_2$ sorption isotherms of PMS-36 after the sixth run catalysis.

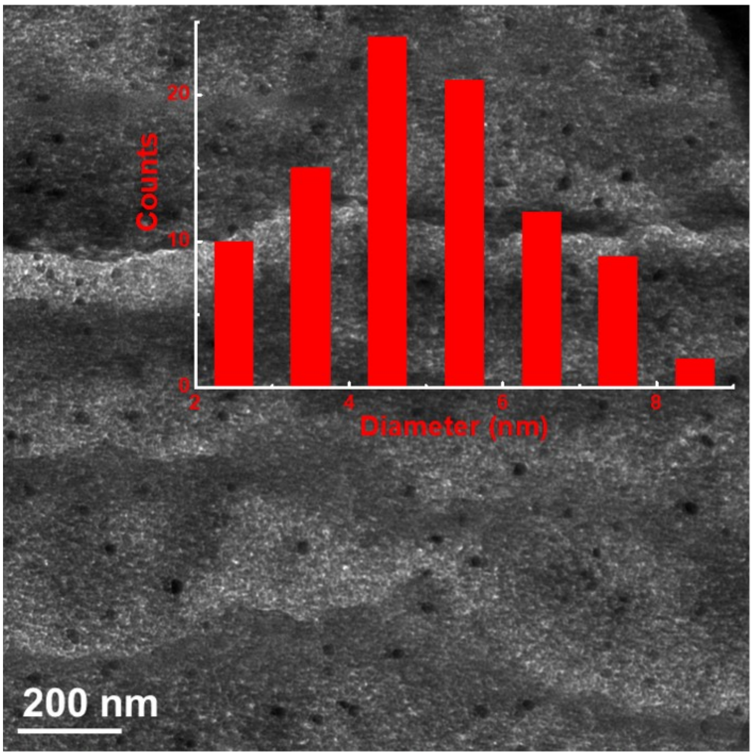

**Fig. S17** HRTEM image of PMS-36 after the sixth run catalysis.

## Tables

**Table S1.** Acidity characterization of PMS materials by Py-IR spectra[a]

| Entry | Ni/Al ratio | Acid sites ($\mu$mol g$^{-1}$) | | |
|---|---|---|---|---|
| | | Brønsted | Lewis | Total |
| 1 | 1.0:0 | 16.3 | 52.7 | 69.0 |
| 2 | 1.0:0.25 | 13.9 | 57.4 | 71.3 |
| 3 | 1.0:0.5 | 18.2 | 61.8 | 80.0 |
| 4 | 1.0:1.0 | 11.6 | 79.3 | 90.9 |
| 5 | 1.0:1.25 | 27.4 | 90.9 | 118.3 |
| 6 | 1.0:1.5 | 28.4 | 94.8 | 123.2 |

[a] Brønsted and Lewis acid site concentrations were determined by integrating the peak areas at 1540 and 1450 cm$^{-1}$ using the molar extinction coefficients of Emeis, respectively.[S1]

**Table S2.** BET surface and pore volumes of the PMS materials with different nickel/silicon ratios

| Entry | Si/Ni | $S_{BET}$ ($m^2/g$) | Pore Volume ($cm^3/g$) |
|---|---|---|---|
| 1 | 3:1 | 206 | 0.46 |
| 2 | 6:1 | 244 | 0.45 |
| 3 | 8:1 | 368 | 0.55 |
| 4 | 10:1 | 266 | 0.59 |

**Table S3.** HDO of guaiacol to cyclohexane catalyzed by the PMS materials with different nickel/silicon ratios[a]

| Entry | Ratio (Ni/Si) | Yield (%)[b] |
|---|---|---|
| 1 | 1:3 | 46 |
| 2 | 1:6 | 83 |
| 3 | 1:8 | >99 |
| 4 | 1:10 | 67 |

[a] Reaction conditions: guaiacol (0.5 mmol), $H_2$ (2.0 MPa), 10 mL of n-dodecane, 200 $^{o}$C, 7 h.

[b] Detected by gas chromatography (GC) with 1,4-dioxane as the internal standard.

**Table S4.** Catalytic results for the transformation of guaiacol to cyclohexane by the literature catalysts

| Entry | Catalyst | T ($^oC$) | TOF ($h^{-1}$) | $P_{H2}$ (MPa) | Conv. (%) | Yield. (%) | Ref. |
|---|---|---|---|---|---|---|---|
| 1 | Pt/zeolite | 250 | - | 4 | >90 | 45.3 | S2 |
| 2 | Pt/Al-SBA-15 | 220 | - | 3 | 100 | 80 | S3 |
| 3 | Pd/C + zeolite | 275 | - | 1.5 | 100 | 0.3 | S4 |
| 4 | Pd/C + $H_3PO_4$ | 250 | - | 5 | 100 | 75.7 | S5 |
| 5 | Ru/$SiO_2$–$Al_2O_3$ | 250 | - | 4 | 100 | 60 | S6 |
| 6 | Pd/WOx/γ-$Al_2O_3$ | 300 | - | 7 | 100 | 88 | S7 |
| 7 | Pt/H-MFI-90 | 180 | - | 5 | 100 | 96 | S8 |
| 8 | Nix-Fey/CNT | 400 | 370.2 | 3 | 96.8 | 80.7 | S9 |
| 9 | Ni/MCM-41+HZSM-5 | 240 | - | 5 | 100 | 84.1 | S10 |
| 10 | NiMo/SBA-15 | 250 | - | 5 | 90 | 56 | S11 |
| 11 | Ni/$SiO_2$–$ZrO_2$ | 300 | - | 5 | 100 | 96.8 | S12 |
| 12 | Ni/$TiO_2$–$ZrO_2$ | 300 | - | 4 | 100 | 86.4 | S13 |
| 13 | Sulfided Ni/W/$TiO_2$ | 300 | - | 7 | 100 | 16 | S14 |
| 14 | PMS-36 | 200 | 50.28 | 2 | >99.9 | >99.9 | This work |

## References

S1 C. A. Emeis, Determination of integrated molar extinction coefficients for infrared absorption bands of pyridine adsorbed on solid acid catalysts, *J. Catal.,* 1993, **141**, 347−354.

S2 E. H. Lee, R. Park, H. Kim, S. H. Park, S.-C. Jung, J.-K. Jeon, S. C. Kim and Y.-K. Park, Hydrodeoxygenation of guaiacol over Pt loaded zeolitic materials, *J. Ind. Eng. Chem.*, 2016, **37**, 18–21.

S3 M. S. Jang, R.-s. Park, I.-G. Lee, J. M. Kwak, Y.-K. Park and C. H. Ko, Catalytic upgrading of lignin derived bio-oil model compound using mesoporous solid catalysts, *Res. Chem. Intermed.*, 2016, **42**, 3–17.

S4 H. Shafaghat, P. S. Rezaei, and W. M. A. W. Daud, Catalytic hydrogenation of phenol, cresol and guaiacol over physically mixed catalysts of Pd/C and zeolite solid acid, *RSC Adv.*, 2015, **5**, 33990–33998.

S5 C. Zhao, Y. Kou, A. A. Lemonidou, X. Li and J. A. Lercher, Highly selective catalytic conversion of phenolic bio-oil to alkanes, *Angew. Chem. Int. Ed.*, 2009, **48**, 3987–3990.

S6 C. R. Lee, J. S. Yoon, Y.-W. Suh, J.-W. Choi, J.-M. Ha, D. J. Suh and Y.-K. Park, Catalytic roles of metals and supports on hydrodeoxygenation of lignin monomer guaiacol, *Catal. Commun.*, 2012, **17**, 54–58.

S7 Y.-K. Hong, D.-W. Lee, H.-J. Eom and K.-Y. Lee, The catalytic activity of Pd/WOx/$\gamma$-$Al_2O_3$ for hydrodeoxygenation of guaiacol, *Appl. Catal., B*, 2014, **150–151**, 438–445.

S8 M. Hellinger, H. W. P. Carvalho, S. Baier, D. Wang, W. Kleist and J. D. Grunwaldt, Catalytic hydrodeoxygenation of guaiacol over platinum supported on metal oxides and zeolites, *Appl. Catal., A*, 2015, **490**, 181–192.

S9 H. Fang, J. Zheng, X. Luo, J. Du, A. Roldan, S. Leoni and Y. Yuan, Product tunable behavior of carbon nanotubes-supported Ni–Fe catalysts for guaiacol hydrodeoxygenation, *Appl. Catal., A*, 2017, **529**, 20–31.

S10 S. Qiu, Y. Xu, Y. Weng, L. Ma and T. Wang, Efficient hydrogenolysis of guaiacol over highly dispersed Ni/MCM-41 catalyst combined with HZSM-5, *Catalysts*, 2016, **6**, 134–149.

S11 B. M. Q. Phan, Q. L. M. Ha, N. P. Le, P. T. Ngo, T. H. Nguyen, T. T. Dang, L. H. Nguyen, D. A. Nguyen and L. C. Luu, Influences of various supports, γ-$Al_2O_3$, $CeO_2$, and SBA-15 on HDO performance of NiMo catalyst, *Catal. Lett.*, 2015, **145**, 662–667.

S12 X. Zhang, Q. Zhang, L. Chen, Y. Xu, T. Wang and L. Ma, Effect of calcination temperature of Ni/$SiO_2$-$ZrO_2$ catalyst on its hydrodeoxygenation of guaiacol, *Chin. J. Catal.*, 2014, **35**, 302–309.

S13 X. Zhang, J. Long, W. Kong, Q. Zhang, L. Chen, T. Wang, L. Ma and Y. Li, Catalytic upgrading of bio-oil over Ni-based catalysts supported on mixed oxides, *Energy Fuels*, 2014, **28**, 2562–2570.

S14 Y.-K. Hong, D.-W. Lee, H.-J. Eom and K.-Y. Lee, The catalytic activity of sulfided Ni/W/$TiO_2$ (anatase) for the hydrodeoxygenation of guaiacol, *J. Mol. Catal. A: Chem.*, 2014, **392**, 241–246.